

## Tidal dynamics and associated features of the northwestern shelf of the Alboran Sea

JESUS M. GARCÍA LAFUENTE\* and NATALIO CANO LUCAYA†

(Received 20 May 1991; in revised form 19 May 1992; accepted 24 August 1992)

**Abstract**—Current meter records from several stations in the northwestern Alboran Sea have been examined, to determine the structure of the tide on the Spanish Continental shelf. Tidal activity is restricted mainly to the westernmost area, where an inflowing jet of Atlantic water through the Strait of Gibraltar is observed almost permanently. A remarkable baroclinic tide, dominated by the interfacial mode, exists in this area. The geographic location of the jet and associated front, which exhibits low frequency fluctuations, controls the intensity of the baroclinic tide: the influence of the spring–neap tidal cycle is also noticeable. A study of the propagation of this internal tide confirms it as a feature related to the density front. During certain tidal cycles, internal hydraulic jumps appear to be formed somewhere over the shelf, shortly after high tide; later, they decay releasing undular internal bores. Internal waves originating from the Gibraltar Strait (generated at Camarinal Sill) are detected regularly at the outer and westernmost station of our study area. All these features become less distinctive in an easterly direction.

### INTRODUCTION

In the analysis of tidal current records, both barotropic and baroclinic tides are superposed. The barotropic part accounts for the periodic sea surface oscillations. Thus, spectral analysis of sea level (or of a purely barotropic tidal current) almost invariably gives amplitude maxima at the existing frequencies in the tide-generating potential; this permits the evaluation of reliable harmonic constants, used for prediction tables.

In the actual tidal currents, baroclinic and barotropic tides may be comparable in intensity. The former is not forced directly by the tide-generating forces, but by interaction between the barotropic tide and bottom topography (BAINES, 1982; OU and MASS, 1988). Its subsequent interaction with the velocity and density fields may distort significantly the periodicities, related usually to sea surface oscillations. The final result, assuming a significant baroclinic tide, is a somewhat intermittent signal without spatial coherence: energy displacements are towards unimportant barotropic lines, or energy spreading around the intense ones. Under these circumstances, harmonic constants cannot be used for reliable predictions.

The local dynamics of our area of study (see Fig. 1) are influenced strongly by the exchange of water through the Strait of Gibraltar: relatively fresh Atlantic water flows into the Mediterranean Sea near the surface, with slightly less salty Mediterranean water

---

\*Department of Applied Physics, University of Málaga, Spain.

†Instituto Español de Oceanografía, Málaga, Spain.

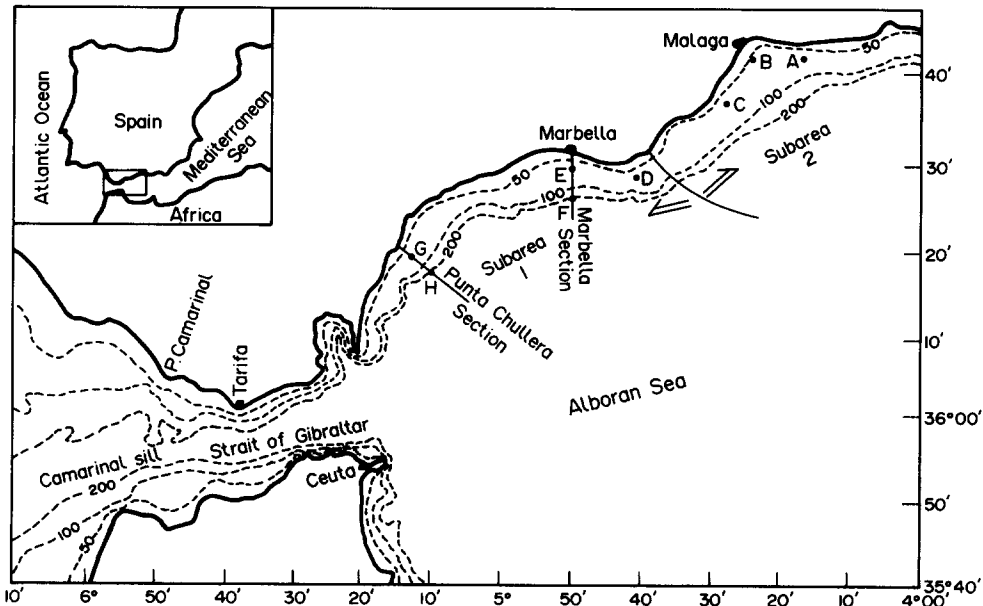


Fig. 1. Map showing the geographic location of all stations. A dotted line separates sub-areas 1 and 2, mentioned in the text.

flowing out near the bottom (because evaporation exceeds precipitation and river discharge in the Mediterranean Sea). The westernmost basin of the Alboran Sea contains usually a large anticyclonic gyre of Atlantic water, sustained by a jet of inflowing water which forms its northern boundary.

Harmonic constants of the tidal currents, evaluated from direct observations of currents at Camarinal Sill (RICO and RUIZ, 1988), are in good agreement with the values calculated using sea level prediction data (barotropic tide) and assuming cross-strait geostrophy (GARCÍA LAFUENTE and ALMAZAN, 1990). The tidal currents in the Strait of Gibraltar are basically, therefore, barotropic and a noticeable barotropic tide is expected in sub-area 1 (see below), close to the Strait. Bottom topography (i.e. the continental slope) and the presence of the jet and associated density front should distort the pattern, however, causing a relatively important baroclinic tide to appear. Sub-area 2, farther away from the Strait, does not show any noticeable tidal activity.

This contribution describes the behaviour of the tide and associated features in sub-area 1, following some general comments on the data and the results provided by standard analysis. The study of the detection and propagation of the baroclinic tide is described, then followed by a discussion of the observations and results.

#### DATA COLLECTION AND ANALYSIS

The data were collected by the Instituto Español de Oceanografía between 1978 and 1980, within the Co-operative Spain-U.S.A. Project No. 3044. Figure 1 shows the location of moorings and Table 1 summarizes their general characteristics. Simultaneous data from Stas E1 and F and from G and H, permit the study of the baroclinic tides. These are

Table 1. General remarks on name of the stations, geographical situation and elapsed time of the moorings studied in this paper

Sta.	Name	Location		Bottom depth	Depth of instrument	From dd/mm/yy	To dd/mm/yy	Sampling interval
		Latitude (N)	Longitude (W)					
A	La Cala	36°41.0	4°17.0	40 m	25 m	22/01/80	20/03/80	10 min
B1	Malaga	36°41.4	4°24.2	32 m	20 m	20/11/79	21/12/79	10 min
B2	Malaga	36°41.4	4°24.2	32 m	17 m	27/02/80	25/04/80	10 min
C	Torremolinos	36°36.5	4°28.2	57 m	17 m	09/11/78	28/11/78	5 min
D	P. Calaburras	36°27.8	4°41.2	60 m	20 m	09/11/78	28/11/78	5 min
E1S	Marbella	36°28.7	4°50.0	60 m	20 m	22/02/79	20/03/79	5 min
E2S	Marbella	36°28.7	4°50.0	60 m	20 m	27/03/79	29/05/79	10 min
E1F	Marbella	36°28.7	4°50.0	60 m	40 m	04/03/79	23/03/79	5 min
E2F	Marbella	36°28.7	4°50.0	60 m	40 m	27/03/79	29/05/79	10 min
FS	Marbella	36°25.2	4°50.0	200 m	10 m	22/02/79	26/03/79	5 min
FF	Marbella	36°25.2	4°50.0	200 m	80 m	22/02/79	26/03/79	5 min
GS	P. Chullera	36°18.6	5°12.8	68 m	28 m	08/05/80	14/06/80	10 min
GF	P. Chullera	36°18.6	5°12.8	68 m	48 m	09/05/80	14/06/80	10 min
HS	P. Chullera	36°16.8	4°10.5	200 m	35 m	07/05/80	02/07/80	10 min
HF	P. Chullera	36°16.8	4°10.5	200 m	115 m	07/05/80	02/07/80	10 min

referred to as the *Marbella* section (MA section) and the *Punta Chullera* section (PC section), respectively.

Mooring F was moved slightly from its theoretical position and the shallower current meter was only 10 or 12 m below the sea surface. This depth was not enough to prevent leakage of energy from waves and swell into the tidal bands, although no “astronomical” energy is likely to have been transmitted to the current meter record. Thus, the high values recorded by it should be considered carefully.

## RESULTS

### *Energy in tidal frequency bands*

Only a small amount of the total energy lies within the tidal bands; of these, the low frequency (sub-inertial) dynamics is the most important. Table 2 summarizes these energy forms for species 1–4. Apart from Sta. G, the total tidal energy everywhere is less than 16%. Absolute values of density of kinetic energy are given in the Table in brackets. From these observations and, for example, the data in Fig. 2, we may conclude:

(i) that tides are negligible in Stas A, B, and C (with a weak signal), located at the Málaga Bight (named sub-area 2), whilst they are noticeable at the remaining stations, located in the area of direct influence of the Strait of Gibraltar (sub-area 1)—thus the spatial differentiation, described by AREVALO and GARCÍA LAFUENTE (1983) for the low frequency dynamics, retains its validity for the tidal dynamics;

(ii) species 2 prevails over all the others, although the diurnal tide may be of some importance—species 3 and 4 are negligible.

The derived  $K_1$  and  $M_2$  harmonic constants are given in Table 3. The lower figures in the “phase” column is a reference value; this is the mean of those given by RICO and RUIZ (1988) at Camarinal Sill for the  $M_2$  together with a theoretical value for  $K_1$  (on the basis

Table 2. Percentage of energy on each tidal band species 1–4, as well as the absolute values (in brackets). Dotted line separates stations of sub-areas 1 and 2

Sta.	Band #1 (0.035–0.045 c h <sup>-1</sup> )		Band #2 (0.075–0.085 c h <sup>-1</sup> )		Band #3 (0.115–0.125 c h <sup>-1</sup> )		Band #4 (0.155–0.165 c h <sup>-1</sup> )		Total (%)
	(%)	(J m <sup>-3</sup> × 10)							
A	1.1	(1.4)	1.9	(2.2)	0.2	(0.2)	0.3	(0.4)	3.5
B2	2.1	(1.2)	1.7	(1.0)	0.5	(0.4)	0.6	(0.4)	5.0
C	2.2	(2.8)	3.5	(4.6)	0.5	(0.6)	0.2	(0.2)	6.4
D	0.5	(1.8)	2.9	(11.8)	0.2	(0.8)	0.2	(0.8)	3.8
E2S	1.5	(2.1)	6.2	(8.9)	0.6	(0.8)	0.5	(0.8)	8.8
E2F	3.8	(2.8)	8.7	(6.2)	0.9	(0.6)	0.6	(0.4)	14.0
FS	1.2	(15.7)	2.9	(35.6)	0.2	(1.8)	0.2	(1.8)	4.5
FF	2.9	(4.4)	11.5	(17.7)	0.6	(1.0)	0.5	(0.8)	15.5
GS	1.7	(2.6)	19.0	(27.2)	0.5	(0.8)	1.1	(1.6)	22.3
GF	2.1	(2.0)	31.5	(30.4)	1.6	(0.6)	1.9	(1.8)	37.1
HS	0.6	(3.0)	2.0	(10.1)	0.1	(0.8)	0.4	(1.8)	3.1
HF	0.6	(2.6)	3.9	(16.2)	0.1	(0.4)	0.1	(0.3)	4.7

that the Strait is a standing wave node for species 1, assuming a cross-strait geostrophic balance between tidal oscillations of the sea surface and the currents).

The phases vary greatly from the reference value. Moreover, the repeated appearance of unexpected amounts of energy, in lines which are not barotropically intense, indicates the presence of an important baroclinic tide.

### *The baroclinic tide*

In order to study baroclinic tides in some detail, it is necessary to know the stability frequency,  $N^2(z) = -(\partial\rho(z)/\partial z)g\rho_0^{-1}$ . In this case, this is not possible because data are available only at two levels. Moreover,  $N^2(z)$  exhibits strong tidal and low frequency variability and the phenomenon has an additional complexity because of its non-linear character. Presented below, however, is a description of the tidal dynamics which should clarify the position, at least over the PC and MA sections.

### *The structure of low-frequency (sub-inertial) density and velocity fields*

The low-passed series of salinity (panel B) and velocity (stick diagrams, panel C) are plotted in Figs 3 and 4 at two depths for the two stations of each section. The A panels outline a mean state: the  $S = 37.5\text{‰}$  isohaline is an interface in a two-layer sea, with lighter Atlantic water ( $S < 37\text{‰}$ ) overlying Mediterranean, denser water ( $S > 38\text{‰}$ ). Throughout this contribution reasons supporting this assumption are presented, which can be relaxed to consider a weakly stratified sea above and below the  $S = 37.5\text{‰}$  surface (with a strong pycnocline in its vicinity). The isohaline may intersect the free surface (GIL, 1988), separating weakly and strongly stratified regions; these are shown as “M” and “S” in panels A.

The interface migrates to shorewards or seawards, diminishing or enlarging the size of

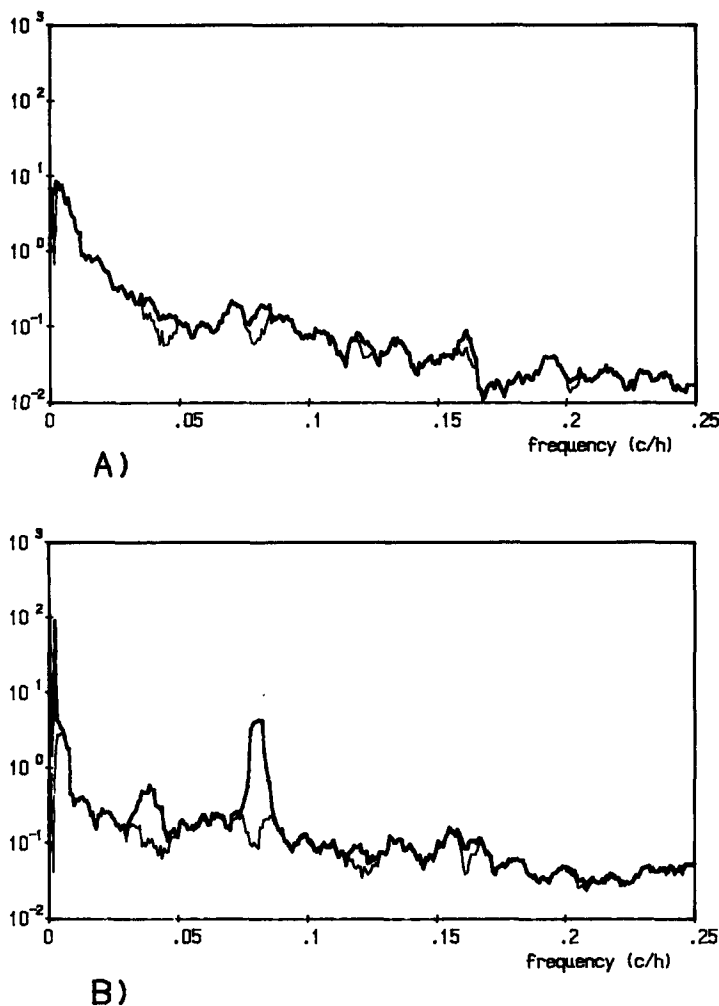


Fig. 2. (A) Energy spectra of currents ( $\text{cm}^2 \text{s}^{-2}$ ) at Sta. B2. (B) As with (A), but for Sta. Hf. In both figures, the heavy line corresponds to the recorded current and the light line to the residual current. (Note: Table 2 indicates 5% of the total energy in tidal bands for both but, whilst the semi-diurnal signal is negligible at B2, Hf shows a clear peak in this band. An obvious reason is the greater low frequency activity at Hf.)

the M region; its slope, sketched in panels A, is a result of geostrophic adjustment of the two-layer flow (panels C). The existence of both the interface and the two-layer flow will be shown to be crucial for the baroclinic tide.

The excursions of the interface are undoubtedly related to the fluctuations in the jet position, which has been reported extensively [GALLAGER *et al.* (1981), CHENEY and DOBLAR (1982)]; this is caused mainly by variability in the inflowing Atlantic water, due to large-scale forcing [HEBURN and LAVIOLETTE (1990)]. The horizontal profile of the velocities of the Atlantic inflow is rather complex, having a central core (or "jet") following more or less the axis of the Strait (with speeds of  $100 \text{ cm s}^{-1}$  or greater) and

Table 3. Harmonic constants for  $M_2$  and  $K_1$  evaluated from the original data in each one of the stations. Dotted line separates sub-areas 1 and 2. The orientation of the current ellipse refers to a Cartesian frame with the x axis eastwards. Letter C (A) means clockwise (anticlockwise) rotation; symbol — is used when the ellipse has degenerated in a straight line. At the bottom of the phase column a reference value, inside brackets, is given

Sta.	Constituent $M_2$					Constituent $K_1$				
	Major Semiaxis ( $\text{cm s}^{-1}$ )	Minor Semiaxis ( $\text{cm s}^{-1}$ )	Orientation major axis ( $^\circ$ )	Phase ( $^\circ$ )	Rotation	Major Semiaxis ( $\text{cm s}^{-1}$ )	Minor Semiaxis ( $\text{cm s}^{-1}$ )	Orientation major axis ( $^\circ$ )	Phase ( $^\circ$ )	Rotation
A	1.1	0.5	355	51	C	1.0	0.5	39	9	A
B1	2.4	0.2	40	42	C	1.4	0.0	8	165	—
B2	0.8	0.4	84	330	A	0.3	0.2	102	232	C
C	4.2	1.9	45	26	C	1.5	1.0	34	83	C
-----										
D	7.3	2.0	22	220	C	2.2	0.2	7	77	C
E1S	2.5	1.7	22	148	A	1.9	0.6	311	313	A
E2S	2.5	1.1	332	138	C	1.1	0.2	24	67	A
E1F	3.5	2.3	65	311	C	2.0	1.2	323	48	C
E2F	3.6	0.1	24	126	C	1.9	1.0	76	86	C
FS	6.1	0.5	4	96	C	6.1	3.5	341	342	C
FF	4.9	0.3	357	91	C	1.8	1.6	22	97	C
GS	8.6	1.6	54	151	A	2.2	0.4	77	50	C
GF	8.1	0.3	15	123	C	2.2	0.3	75	49	C
HS	4.2	2.6	350	218	A	2.3	0.4	6	137	C
HF	7.5	0.1	19	170	C	1.8	0.0	50	81	—
				(140)					(140)	

surrounded by other and slower secondary cores (PERKINS *et al.*, 1990). It seems that Stas H and, eventually, F are located in the northernmost part of the core (northern core). Reasons are presented below to confirm this statement.

As it can be seen in Fig. 4, the interface was very close to the shoreline by 25 February 1979; perhaps, at this time, it did not intersect even the free surface. Stations Es and Fs showed typical Atlantic values of salinity ( $\approx 36.5\text{‰}$ ), while Ff was in Mediterranean water ( $\approx 38\text{‰}$ ). A noticeable two-layer, sheared flow was detected at F. Unfortunately, there were no data from Ef to complete the description. Afterwards, the jet migrated to the south, leaving Sta. Es within Mediterranean water on around 4 March 1979. Two days later the same situation occurred with Fs. Simultaneously, the baroclinic structure of velocities disappeared at Stas F and, after 7 March 1979, the current became basically barotropic. An exception is the brief period around 12 March 1979, when Fs registered salinity values less than  $37.5\text{‰}$  again; consequently, the baroclinic structure appeared. By the end of the record, the interface was rapidly approaching the shoreline.

The same fluctuating behaviour was observed in the PC section, but was less in amplitude. The orientation of the coastline seems to be the most obvious reason for this pattern, although differences in general meteorological conditions (moorings E1–F and G–H are not simultaneous) could have accounted partially for the discrepancies. Throughout the periods of the moorings, Sta. H was located always in the northern core, but G was never located there.

In general, the salinities at Hs and Fs are not purely Atlantic ( $S \leq 36.5\text{‰}$ ) in character,

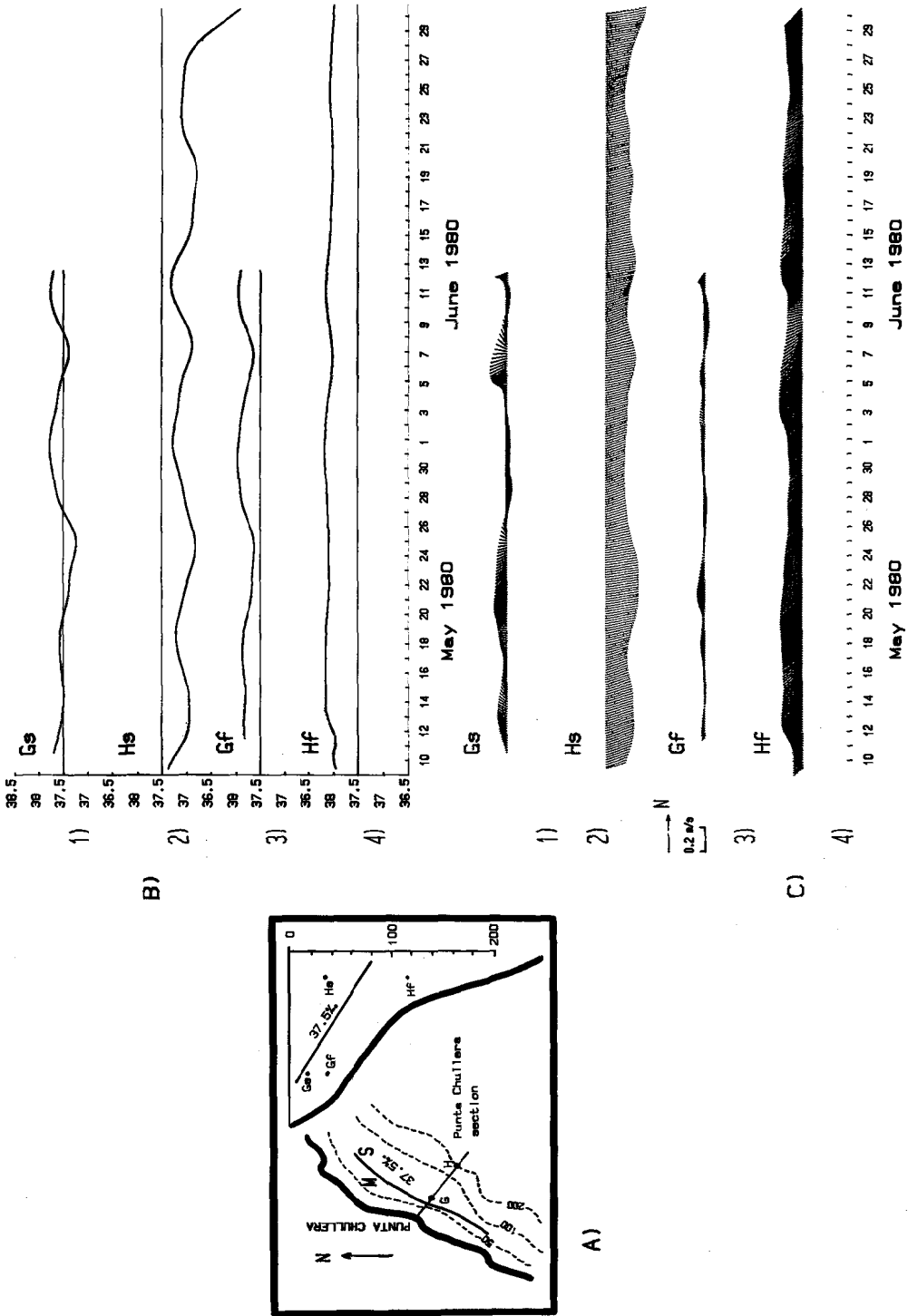


Fig. 3. (A) Sketch of the PC section, showing the position of the stations and a mean location of the  $S = 37.5\text{‰}$  isohaline. (B) Low-pass time-series of salinity. (C) Low-pass stick diagram of velocity.

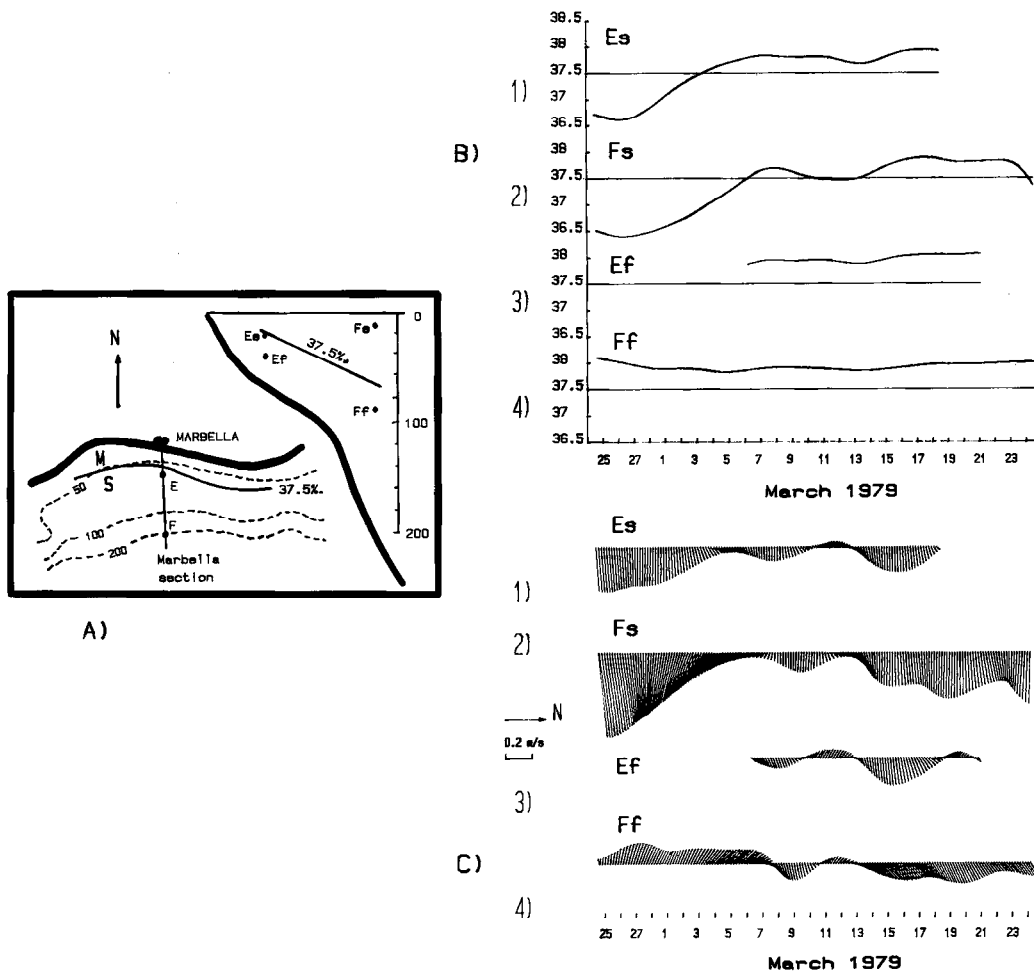


Fig. 4. *Idem* as Fig. 3, for MA section.

neither are they purely Mediterranean at Hf and Ff ( $S \approx 38.5\text{‰}$ ); this denotes the presence of mixed waters, because these stations are close to the northern boundary of the northern core where mixing processes (partially due to tidal activity) must be of some importance. A decrease in salinity at Hs would be detected when the northern core approaches the shore. Assuming a horizontal profile of velocity in the core, with a maximum along its axis and decreasing outwards along both boundaries, such an approach implies a greater velocity at Hs; this is in agreement with observations. On the basis of continuity, the velocity within the lower layer will also increase. This explains why the speeds at both levels tend to change in phase, contrary to what happens in an ideal two-layer baroclinic flow. In the latter, an increase in the upper layer thickness (i.e. the salinity at Hs diminishes) is followed by an increase of velocity in the lower one, but a decrease in the upper layer.

It should be noted that there is a 9–12 day pseudo-periodicity, shown in Fig. 3, which has been reported as a typical time-variability of the jet location by some authors (PERKINS *et al.*, 1990).

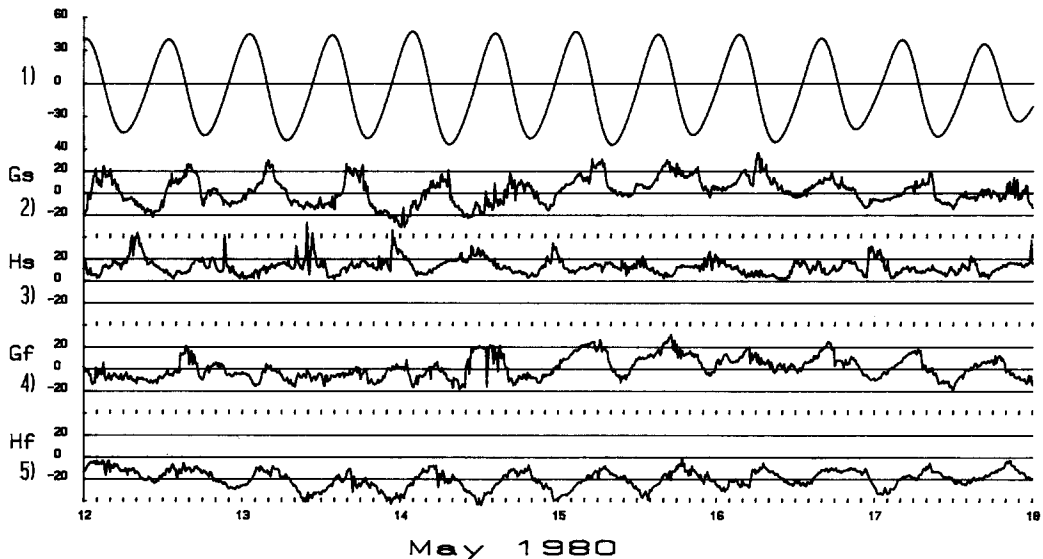


Fig. 5. Alongshore component of the velocity ( $\text{cm s}^{-1}$ ), positive eastwards, into the Alboran Sea, at the PC section (panels 2–5). Panel 1 is the predicted sea level at Ceuta.

### *Punta Chullera section*

The tide in the western Mediterranean Sea is forced mainly by the Atlantic tide through the Strait of Gibraltar, with the free tide being negligible. As it behaves like a standing wave, barotropic tidal current flows into the Mediterranean Sea when the tide is falling and *vice versa*. These features, transported by the jet, should be detected when examining the alongshore component of velocity ( $V_L$ ), since the jet flows parallel to the shore. Figure 5 shows these components over a few days at the four stations along the section, together with the predicted tidal heights at Ceuta. It can be seen that the condition for a standing wave (i.e. a barotropic tide) is verified regularly at Hf, but not at Stas G or Hs. In other words, the tide is mainly barotropic at Hf, but must have an appreciable baroclinic component at the other stations (the tidal current at Hf is slightly delayed however, from its theoretical behaviour. For example, Table 3 shows a highly polarized  $M_2$  tidal current, which is the prevailing constituent, at this station with a phase value  $30^\circ$  greater than expected. This (1 h) delay is seen easily in Fig. 5; it might be due to the lateral momentum transfer from the axis of the jet, with the current behaving theoretically here, towards the boundaries.

Figure 6 shows salinities and stick diagrams representing velocities at the four stations. Some peculiarities are seen readily: (1) extensive microstructure especially at Stas G and Hs—the closer the salinity is to  $37.5\text{‰}$  the more pronounced is the microstructure; (2) negative correlation between the salinity at Hs and the remainder of the stations; (3) the intermittent step-like structure of the salinity measured at Sta. G—related to the low-frequency velocity, to the location of the interface and to the spring–neap tidal cycle (it should be noted how this structure disappears when the flow is weak, coincidental with a withdrawal of the interface (25–30 May) on neap tides); and (4) the intermittent and well-

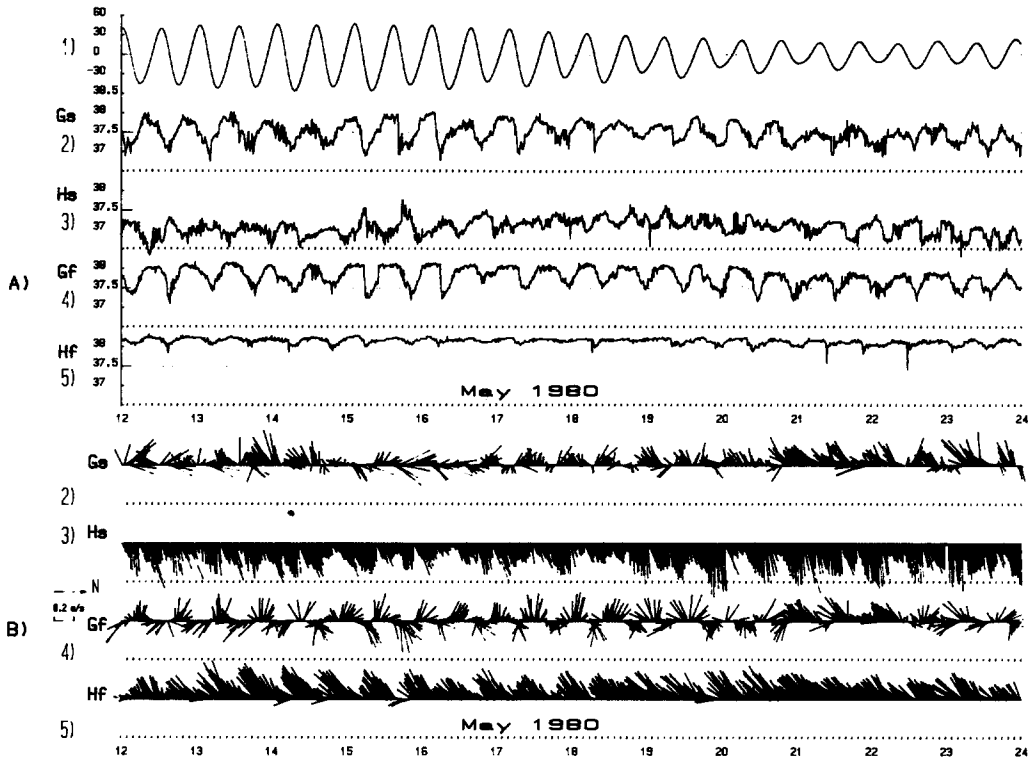


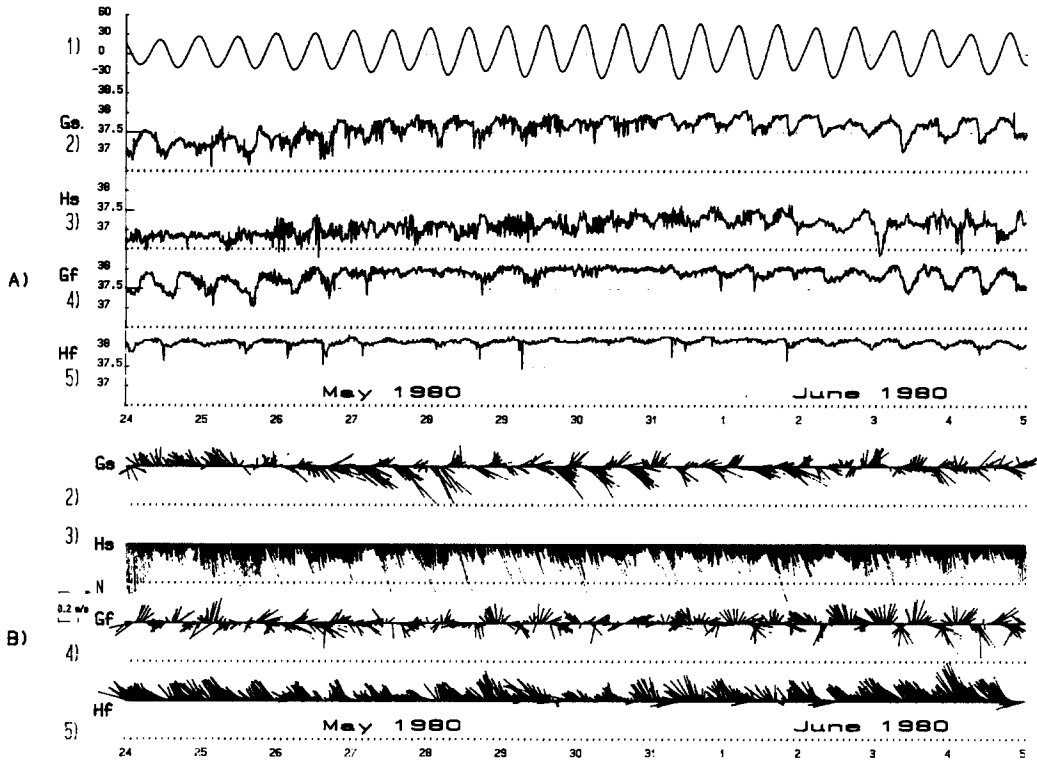
Fig. 6. (A) Salinities at the stations of the PC section with the predicted level at Ceuta on top. (B) Stick diagrams.

defined sudden changes in both speed and direction of the current at Hs (25 May–4 June), which do not show in the data from the remainder of the stations.

In order to comment on these phenomena, it should be noted that the sampling interval used (in both time and spatial intervals) does not permit a satisfactory investigation of the microstructure. Nonetheless the behaviour described below is deduced from a reasonable accumulation of traces, but more detailed sampling is needed to provide further confirmation. With the sampling strategy used here, only some of the phenomena are detected successfully.

Figure 7 shows salinities and onshore velocities  $V_N$  (the significant component for baroclinic tides) during the same period as represented by Fig. 5. During the rising tide, barotropic forcing increases  $V_L$  towards the Strait and  $V_N$  shorewards within the lower layer (i.e. at Hf); this carries Mediterranean water to the shelf, piling it up against the continental slope. Such an arrival moves the lighter water of the surface layer on the shelf in an offshore direction; this is seen by the lower salinity values and seawards increase in  $V_N$  registered at Hs. At the same time, the salinity increases at both stations at G and the interface steepens its slope; this may be large, but is not supported geostrophically.

On the other hand, the intrusion of the Mediterranean waters onto the shelf allows the jet to approach the shoreline to refill the space left by that water. Thus,  $V_L$  increases also at Hs as well; this is because of the horizontal profile of velocities associated with the jet,

Fig. 6. *Continued.*

mentioned previously. This is an unexpected result since barotropic forcing should decrease the current speed at Hs on the rising tide. Figure 5 shows clearly, however, the trend of  $V_L$  to increase or decrease simultaneously at Hs and Hf. This behaviour implies the existence of upwelling over the shelf and weak fluctuation of the location of the jet, both with a tidal periodicity.

During the ebb tide, barotropic forcing diminishes the speed of the currents in the lower layers, allowing the interface to relax its slope and compelling the jet to withdraw. Thus,  $V_L$  decreases at both H stations, whilst  $V_N$  reverses at Stas Gf and Hf (but, surprisingly, not at Gs) in order to evacuate the Mediterranean water. Consequently, their salinities decrease, whilst increasing at Hs. This characteristic, together with those on the rising tide, explains the negative correlation between salinities at Hs and the other stations.

Figure 7 confirms that, in general terms, the behaviour is as described. Other peculiarities, such as the absence of a reversal of  $V_N$  at Gs, are described and discussed below.

**Internal hydraulic jump.** Figure 8 presents a series of abstracts from data set at different stages of the tidal cycle, commencing with low water on 15 May (at 0800 h). All the representations have been made up from data taken from Figs 5 and 7. The interface location shown is approximate.

The sequence of abstracts corresponding to the rising tide confirms the behaviour depicted above, although the dynamics appears now to be more energetic. It can be seen

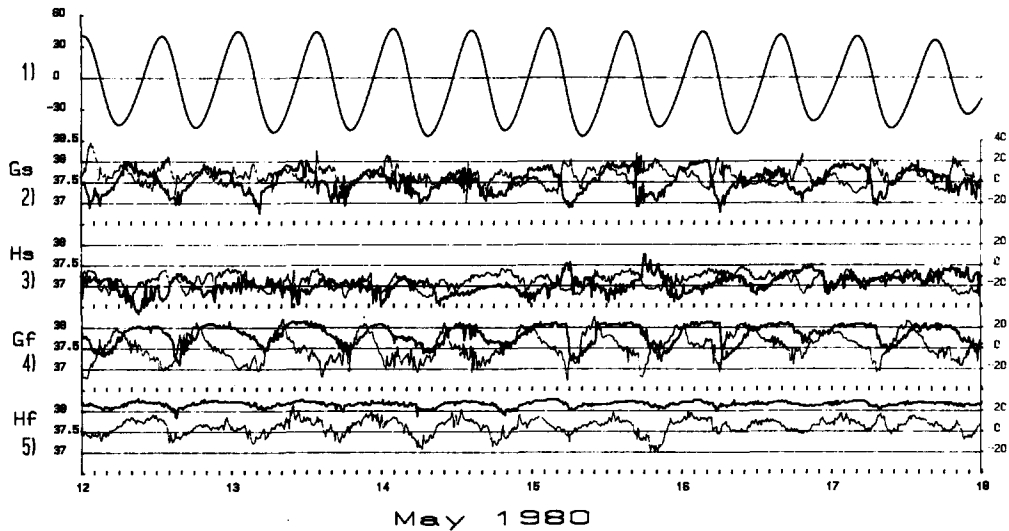
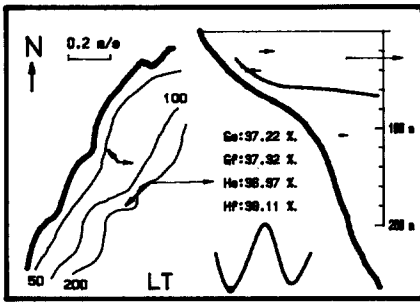


Fig. 7. Salinity (heavy line, left-hand scale) and onshore velocity (light line, right-hand scale in cm, positive shorewards) at the PC section, for the same period as shown in Fig. 5. Notice the clear step-like structure of salinities at Sta. G on 15 May, when the formation of an internal hydraulic jump has been postulated.

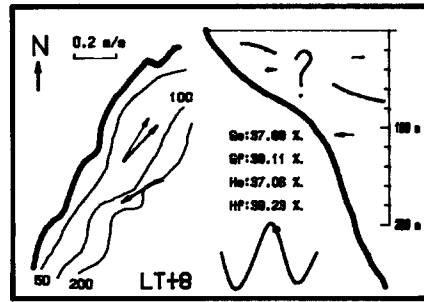
that an increase in velocity at Hf accumulates Mediterranean water against the continental slope and shelf, steepening the interface. Between LT + 4 h and LT + 6 h the salinities at Gs and Gf are similar, whilst it reaches a minimum at Hs. The steep slope of the interface between G and H, sustained by the strong current in the lower layers could be related to an internal hydraulic jump. From LT + 6 h, the current decreases; when it cannot sustain the internal hydraulic jump, this degenerates and releases two internal undular bores around LT + 6 h to LT + 8 h [Fig. 8(D) and (E)]; one is of light water progressing onshore, whilst the other is of denser water moving offshore. Shortly after LT + 8 h, a sudden fall in salinity, followed by noticeable oscillations of the interface, is detected at Gs. An abrupt increase shorewards in  $V_N$ , followed by oscillations related to those of salinity is registered simultaneously [Fig. 8(F)]. This is due probably to the passage of the internal bore and subsequent wave packet past Gs. Rapidly, the same sudden reduction in salinity and oscillations are detected at Gf. Some minutes before,  $V_N$  had increased abruptly to seawards [Fig. 8(G)]; this could be the signature of the denser internal bore released at this station, which is flooded with relatively light water. Salinity and offshore velocity are increased suddenly at Hs, when the bore reaches this station. Barotropic forcing has almost disappeared around LT + 6 h or LT + 7 h. From LT + 12 h, a new cycle begins which may or may not generate another internal hydraulic jump.

The step-like structure in salinity (Fig. 6) is related closely to this phenomenon. The

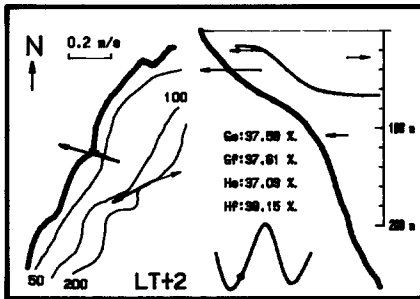
Fig. 8. Sketch of the evolution of the salinity and velocity fields over the tidal cycle of 15 May, starting from 0800 h, at the PC section. The stage of the tide for each abstract is shown at the bottom (starting from low tide, LT). Values of the salinity at these times are shown and velocity vectors drawn in plan view on the left-hand side (the deeper stations with a heavy line). Onshore velocities are shown also on the right-hand side, together with the likely location of the interface. All the values have been deduced from those on Fig. 7.



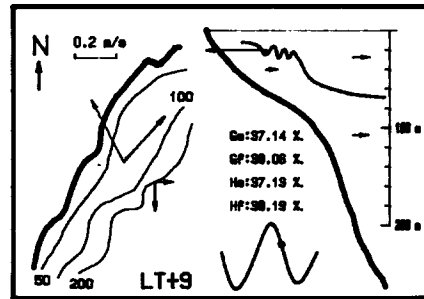
A)



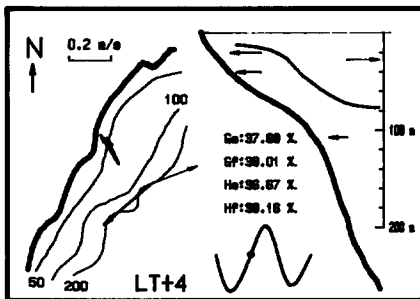
E)



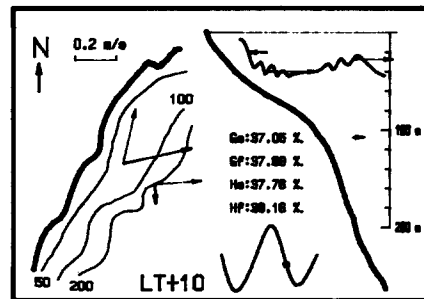
B)



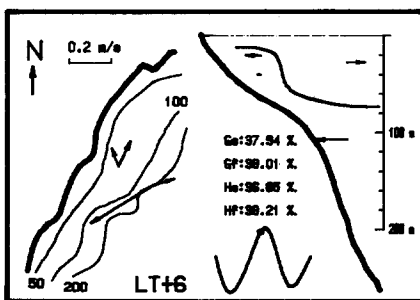
F)



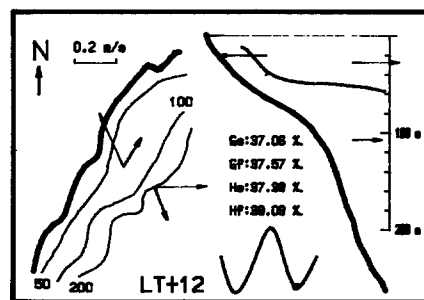
C)



G)



D)



H)

sudden increase in  $V_N$  to shorewards [seawards at Gs (Gf)], simultaneously or immediately before the step decay, support the hypothesis of hydraulic jump formation. Examination of the records proves that the most favourable conditions for its formation during the tidal cycle are as described above. The previous and subsequent cycles appear to create favourable conditions as well. Nevertheless, it cannot be concluded that these hydraulic jumps are formed regularly due to the deficient sampling interval. If the jump is not very pronounced, it may or may not decay as a series of internal bores. If it decays as internal bores it may not be so energetic; hence,  $H_s$  remains insensitive to them but it could be detected at Gs and Gf. No indications of the generation of the jump appear to exist during most of the records. It should be noted, nonetheless, that there is a greater possibility of formation with spring tides, during high/low frequency currents and when the interface is close to the stations at G. These are discussed below.

*Internal waves.* Another remarkable feature of the data set is the isolated peaks in the current, coinciding with slight but sudden changes of direction and density perturbations which take place at  $H_s$ . They are intermittent in nature and occur always about 1–3 h after low tide (i.e. 7–9 h after the previous high water). These features are not detected at the other stations and would correspond to the passage of the internal bore and subsequent internal wave packet, released at Camarinal Sill in the Strait of Gibraltar (see Fig. 1), which propagate eastwards into the Alboran Sea and are advected by the jet. This particular release occurs around high water (HW – 1 h to HW + 1 h, see ARMI and FARMER, 1988; FARMER and ARMI, 1988) less frequently on neap tides.

The phase speed of the waves can exceed 2 or even  $2.5 \text{ m s}^{-2}$  (LAVIOLETTE and LACOMBE, 1988; WATSON and ROBINSON, 1990); this gives an elapsed time of 8–9 h to arrive to Sta. H, 70 km from the Camarinal Sill. Most of the energy propagates along the axis of the jet and only diffracted and low energy rays onto the mean current would arrive at Sta. H. Their arrival is associated with a change in current direction and speed. Because they are bound to the interface and because of their low energy, they are not detected at Stas G. Likewise, they may not be detected at  $H_s$ , unless this station is close to the interface (between 26 May and 2 June, for example). Following the peak in current speed at  $H_s$  there is a lesser oscillation in salinity; this supports the concept that these phenomena are the signature of the passage of the strong internal bore, released at Camarinal Sill.

It should be noted that these internal waves are orthogonal to those associated with the decay of the internal hydraulic jump, which propagates normal to the shoreline. Moreover, they occur at different moments during the tidal cycle, so there is no possibility of confusion between the two mechanisms.

### *Marbella section*

The migration of the jet and associated cores, towards the south, is the most outstanding feature and is responsible for the measurements at this section. Barotropic forcing is less than at the PC section; therefore, all the phenomena will be more closely bound to the interface (i.e. being excluded from the sampling programme).

Figure 9(A) shows a section of the record, 7 days long and commencing on 26 February 1979. Tidal activity increases at the different stations as the northern core moves southward through them (see Sta. Es, between 1 and 3 March). The two “step-like”

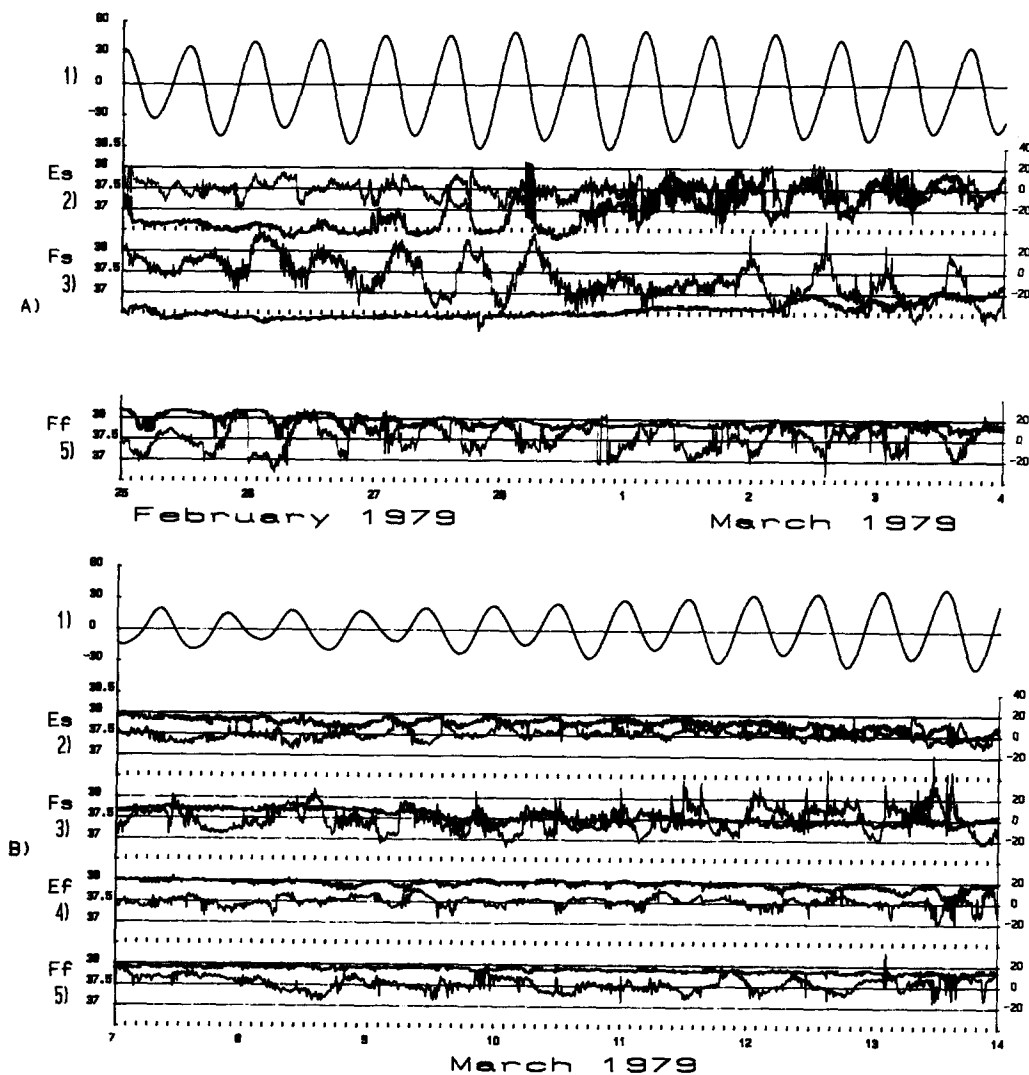


Fig. 9. As Fig. 7, for the MA section during two different periods. Notice a greater activity in Fig. 9(A) corresponding to the first period (when there are no data available from Sta. Ef).

structures in salinity on 28 February, likely to be related internal hydraulic jumps, may have indicated the imminent arrival of the interface a day later. Once the Core has passed, such activity disappears almost everywhere, leaving all the stations in the well-mixed region [see Fig. 9(B)].

The failure of the current meter at Ef and the incorrect location of that at Fs makes it difficult to provide a detailed description of the characteristic here. An important conclusion can be drawn here though, that most of the energy is located in the neighbourhood of the interface. Hence when this is to the south of Sta. F, tidal activity is unimportant over the mixed area. Thus, the interfacial mode dominates the baroclinic tide.

### *Propagation of the baroclinic tide*

The qualitative behaviour of the tide has been described above the terms of particular episodes, rather than the series as a whole. This problem will now be analysed using the mathematical model developed by LEVINE and RICHMAN (1989). The theoretical background to the analysis and details of mathematical procedures can be found there.

The concept is now described briefly. If there is a baroclinic or internal tide, the hodograph of its velocity vector would describe an ellipse which rotates clockwise in the northern hemisphere. The major axis would be oriented along the axis of propagation and the ratio of the major to minor axis is described in terms of  $\sigma/f$  ( $\sigma$  is the tidal frequency,  $f$  the Coriolis parameter). On the other hand, any hodograph can be decomposed into the sum of two counter-rotating ellipses, with both the major axes oriented at a given angle and with a ratio major to minor axis fixed. On the basis of these assumptions, this decomposition is unique. The clockwise rotating ellipse can then be identified with the baroclinic tide and the anticlockwise with "noise". The orientation angle which provides the highest value of the ratio of both the major axes (analogous to the signal-to-noise ratio) is taken as the angle of propagation. This elliptical decomposition has been derived for the four stations of each section, on the basis of difference in horizontal velocity recorded by the upper and lower instrument of each mooring (in order to remove the barotropic part of the velocity field). Prior to this all series were band-pass filtered, to isolate the semi-diurnal frequency  $\sigma$  in the ratio  $\sigma/f$ .

Figure 10(A)–(C) shows the results of the analysis for Stas F, G and H. These data confirm that the presence of the interface is fundamental to the creation of all intense baroclinic signal. This observation is especially clear in Fig. 10(A) (which must be examined with Fig. 4): when the jet migrates southwards and is located away from Sta. F, the signal is greatly reduced. In contrast, a strong signal is found whenever the interface passes through Sta. F. As seen in the bottom panel of Fig. 4, the propagation angle is nearly  $90^\circ$  (i.e. normal to the shoreline, as theory predicts) when the signal/noise ratio is high.

In spite of the weakness in the baroclinic signal at Sta. H, there appears to be a relationship between it and spring tides [Fig. 10(C)]. Probably, spring tides are responsible also for the baroclinic signal at F from 14 March 1979 until the end of the record and they help to intensify the signal by its commencement [Fig. 10(A)]. The signal is clearly baroclinic at Stas G [Fig. 10(B)] and is more or less intense depending upon the location of the interface during the spring–neap tidal cycle. It is interesting to note clockwise rotation of the velocity vectors at Stas G, in the abstracts shown in Fig. 8; this is an almost permanent feature at Gf [Fig. 6(B)]. The angle of propagation lies between  $90^\circ$  and  $135^\circ$  at Sta. G, which is very close to the onshore direction.

## DISCUSSION

It has been demonstrated that the baroclinic tide is important in sub-area 1. The presence of the northern core of the jet and its related density front is fundamental, however, to the existence of a clearly defined baroclinic tide. The closer to the Strait, the more noticeable and persistent the baroclinic signal at the shelf station appears.

Internal hydraulic jumps, formed on the continental shelf at particular times during tidal cycles, are not found infrequently in places with intense baroclinic tides (see HOLLOWAY,

1987; SMYTH and HOLLOWAY, 1988). Such features may decay, releasing internal bores: one propagating seawards, which may be “leaked” into the deeper denser layer at one or two wavelengths (BAINES, 1982); the other progressing shorewards on the shelf, where its features may be emphasized as it proceeds into shallower areas (CAIRNS, 1967).

The internal hydraulic jump appears to be formed at about LT + 6 h, somewhere between Stas G and H (Fig. 8). In terms of the  $V_N$  component of velocity, the jump will be formed when the flow changes from supercritical to subcritical. Figure 11, which is a reproduction of Fig. 8(D), helps to understand what then follows. In a two-layer ocean the condition for critical flow is given by

$$F^2 = F_1^2 + F_2^2 = 1,$$

where  $F$  is a composite Froude number and  $F_i$  the internal Froude number for the upper (1) and lower (2) layers, defined as

$$F_i^2 = \frac{V_{Ni}^2}{h_i g'}$$

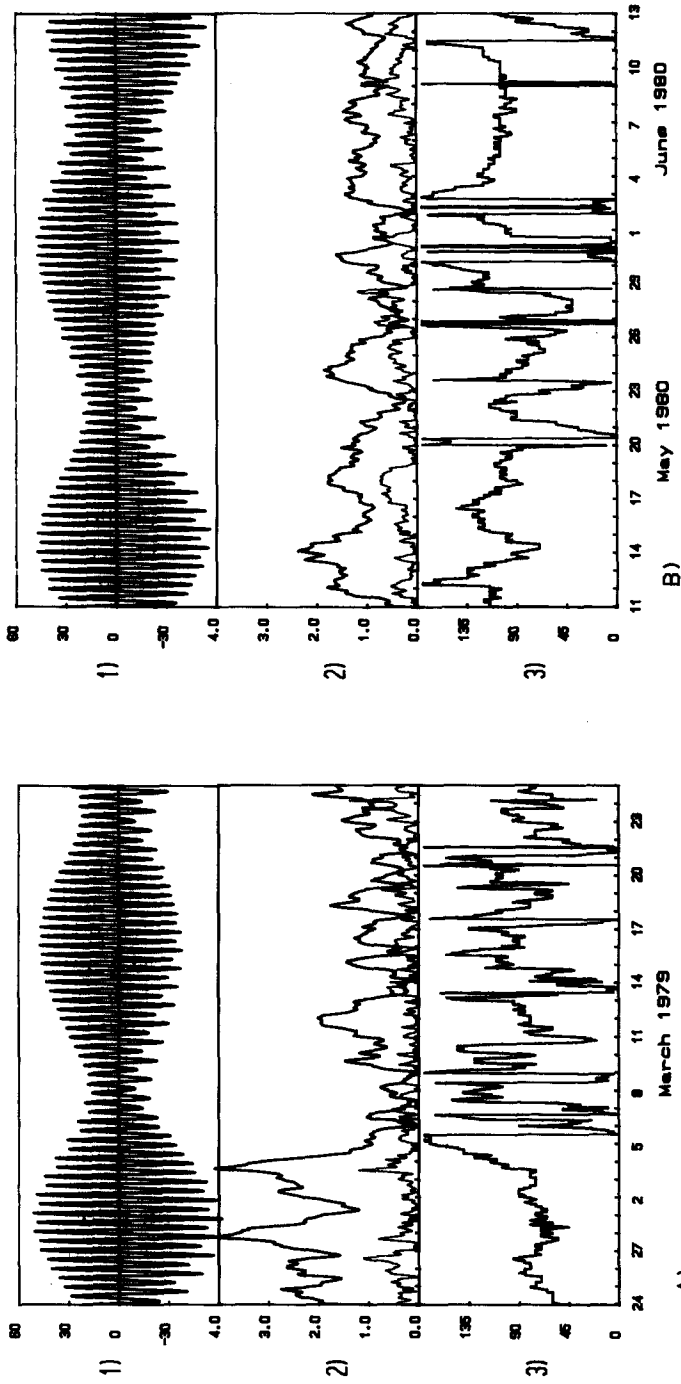
with  $h_i$  and  $\rho_i$  the thickness and density of layer  $i$ ,  $g' = \rho^{-1}g\Delta\rho$  the reduced gravity (with  $\Delta\rho = \rho_2 - \rho_1 \approx 1 \text{ kg m}^{-3}$ ,  $g' \approx 10^{-2} \text{ m s}^{-2}$ ). Although the position of the interface shown in Fig. 11 is only approximate (and, therefore, the values of  $h_i$ ), the flow is clearly subcritical ( $F < 1$ ) in profiles H and G. Flow within the lower layer will be accelerated spatially as it progresses shorewards from Sta. H, because of the bottom topography; this is especially characteristic in water depths of about 100 m, where the bottom slope increases abruptly (in fact, the 100 m isobath may be considered as the outer limit of the continental shelf). If such is the case, it may become supercritical beyond, for example, section I; it would remain in this condition until section II, becoming subcritical again beyond this second critical section. Adjustment from a low (supercritical) to a high stage (subcritical) would be made through an internal hydraulic jump.

If the sketch depicted above is correct, then not only the strength of the barotropic forcing (related to the spring–neap tidal cycle) and the low-frequency current, but the proximity of the interface to the shoreline must be crucial for jump formation. From the data presented above, the higher the salinity at Gs the closer the interface will be to the shoreline [i.e. from the beginning of the record until 20 May 1989 and from 27 May 1980 to 6 June 1980 (Fig. 3)]. Spring tides occurred between 13 and 17 May and between 28 May to 2 June [Fig. 10(B)]; the first of these were the more intense. At  $Hf$  low frequency currents between 14 and 18 May were slightly stronger than those during the first days of June. Thus, conditions suitable for the formation of the jump are found on 15 May. By the end of May and the beginning of June, conditions were also favourable, but to a lesser extent. The existence of “step-like” structures in the salinity at both stations on those days was not surprising: most likely, they corresponded to small internal hydraulic jumps, which were not well monitored by the sampling programme.

In a two-layer ocean, neglecting the rotation of the Earth, the velocity of the progress of an internal wave, whose wavelength is long compared with the water depth is given (SVERDRUP *et al.*, 1942) by

$$c = \left[ \frac{h_1 h_2}{h_1 + h_2} g' \right]^{\frac{1}{2}}.$$

This equation permits the velocity of the progress of the bores to be estimated. On the high side of the jump (i.e. to shorewards),  $h_1 \approx 10 \text{ m}$ ; on its lower side,  $h_1$  is badly defined



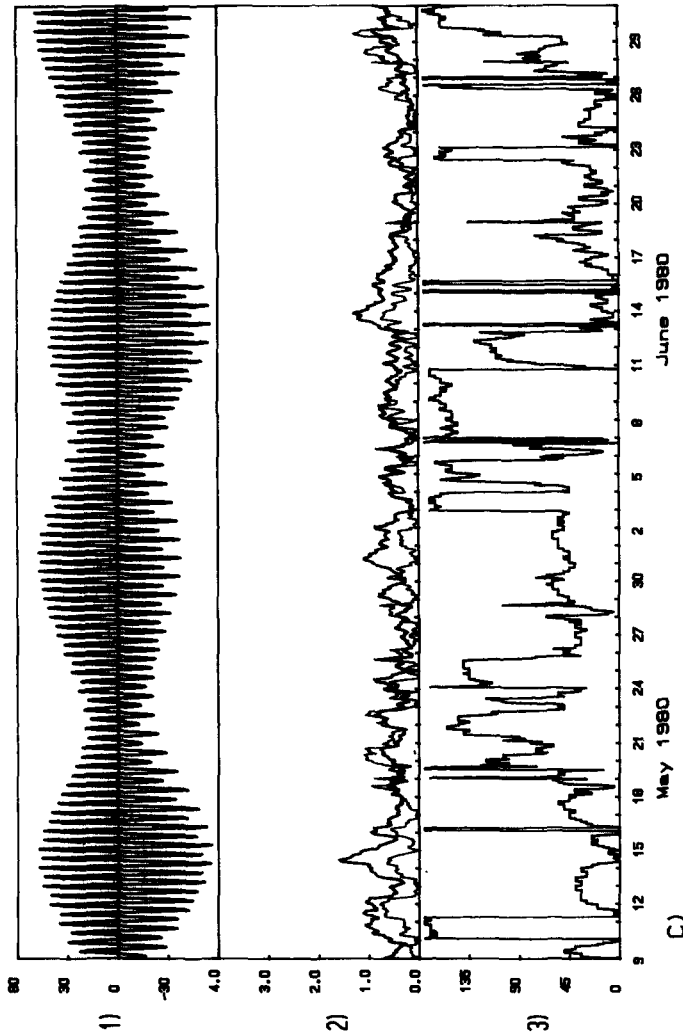


Fig. 10. (A) Result of the analyses of baroclinic tide propagation at Sta F. Panel 1 is the predicted sea level at Ceuta. Panel 2 is the semi-amplitude of major axes of the clockwise (heavy line) and the anticlockwise (light line) hodographs, in  $\text{cm s}^{-1}$ . A strong baroclinic signal implies a much greater value of the first over the second. Panel 3 is the propagation angle,  $0^\circ$  eastwards. (B) *Idem* Sta. G. (C) *Idem* Sta. H.

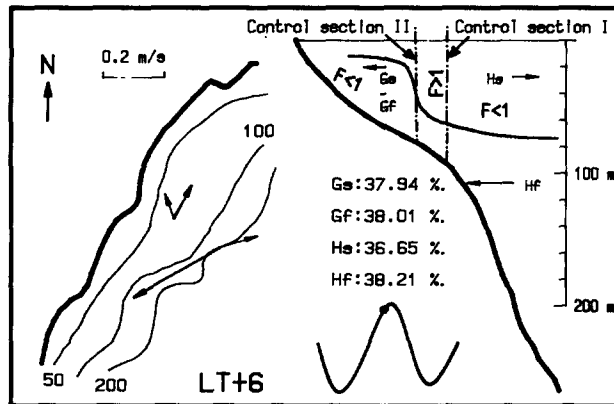


Fig. 11. Sketch of PC section showing the likely mechanism of the internal hydraulic jump formation. Subcritical deeper flow at Hf will become supercritical beyond control section I (because of spatial acceleration); it will remain at this stage until control section II, beyond which it will become subcritical again. The jump will match these two stages.

and perhaps ranges from 40 to 70 m. The bottom depth changes from 60 m to 70–80 m between Sta. G and the location of the formation of the jump (i.e. from 200 to 70–80 m for Sta. H), so that a unique bore velocity cannot be evaluated. However,  $0.3 \text{ m s}^{-1}$  and  $0.5 \text{ m s}^{-1}$  are adequate mean velocities for each of them. Station H is located 5.5 km from Sta. G and the bore proceeding shorewards, arrives at G an hour before the bore propagating seawards arrives at H. The analysis is appropriate if it is assumed that the release of the bores takes place 1.5 km away from Sta. G (i.e. 4 km from H), some 1.5 h before the former is detected at G (LT + 8.5 h) i.e. around LT + 7 h [Fig. 8(D) and (E)] this coincides approximately with a reduction in the barotropic forcing. Thus, the place of formation (outlined correctly in Fig. 11) is on the shelf, near to Sta. G. The 4 km between Stas G and H appears to be sufficient for the bore, in progressing seawards, to be absorbed by the deeper layers. Such a bore will not usually be detected at Sta. H, but is better observed at Sta. G.

On occasions, the rising tide appears to enter the shelf as an internal bore of dense Mediterranean water, which is detected clearly at Gf [the tidal cycle displayed in Fig. 8(B) reflects one such event]. This bore can be detected just a few hundred m away from the shoreline; it is identified by the sudden arrival of saltier, colder and, in particular, turbid water (because of its high content of suspended particles).

There are obvious differences between the oceanographic characteristics of the PC and MA sections. For example, the internal waves coming from the Strait are detected regularly at PC (much more frequently than the hydraulic jump) and never at MA, although such waves have been reported to the southeast of it. At PC, the baroclinic activity is restricted mainly to the region from Sta. H to the shoreline: the amount of activity recorded at H itself being rather low. Similar behaviour might be expected for the MA section, with Stas F and E replacing Stas H and G respectively. There is some evidence to suggest that this situation occurs, but, on the basis of the data set described here, there is more baroclinic activity at F than at E. The reason could be the coastline orientation which implies more barotropic forcing at Hf and, consequently a greater baroclinic response at G. [Note: the failure of the current meter at Ef did not permit confirmation of this.

Analysis of data from the second mooring at Sta. E (i.e. Sta. E2) showed greater baroclinic activity than at the first mooring; there was still less than at G. Unfortunately, however, the second mooring at F was lost.]

Another noticeable difference between the two sections is the greater low-frequency variability at MA in comparison to PC. Three possible explanations could account for this pattern: (1) the different orientations of the shoreline; (2) the distance of each section from the Strait of Gibraltar; and (3) different atmospheric conditions and oceanic circumstances, occasioned by seasonal and very low frequency variability in the oceanic dynamics. When the northern core is to the south of F, the stations within this section are included in sub-area 2, where atmospheric forcing (mainly wind stress) imposes the dynamics.

*Acknowledgements*—This work has been carried out within the framework of co-operation between Málaga University and the Instituto Español de Oceanografía, for the study of oceanographic data collected by the latter Institution over the Spanish continental shelf and slope of the Alboran Sea. We are grateful to colleagues who read and commented on the manuscript; especially to Gregorio Parrilla, Maria Jesús García and Jesús Carretero for assisting us in the analysis of data.

#### REFERENCES

- AREVALO L. and J. GARCIA LAFUENTE (1983) Corrientes en la costa de Málaga: métodos y resultados. *Informes técnicos Instituto Español de Oceanografía*, **13**, 45 pp.
- ARMI L. and D. FARMER (1988) The flow of Mediterranean water through the Strait of Gibraltar. *Progress in Oceanography*, **21**, 1–106.
- BAINES P. G. (1982) On internal tides generation models. *Deep-Sea Research*, **29**, 307–338.
- CAIRNS J. L. (1967) Assymetry of internal tidal waves in shallow coastal waters. *Journal of Geophysical Research*, **72**, 3563–3565.
- FARMER D and L. ARMI (1988) The flow of Atlantic water through the Strait of Gibraltar. *Progress in Oceanography*, **21**, 1–106.
- GALLAGER J. J., M. FECHER and J. GORMAN (1981) Project Huelva.—Oceanographic/acoustic investigation of the western Alboran Sea. *NUSC Technical Report*, **6033**, 109 pp.
- GARCIA LAFUENTE J. and J. L. ALMAZAN (1990) La marea en el Estrecho de Gibraltar. *Proceedings, Workshop on Oceanography of the Strait of Gibraltar*. Marrakech.
- GIL J. (1988) Variación estacional del espesor de la capa de procedencia Atlántica y la formación de agua de invierno en la costa Sur-Occidental Mediterránea. *Informes técnicos Instituto Español de Oceanografía*, **56**, 16 pp.
- HEBURN G. W. and P. E. LAVIOLETTE (1990) Variation in the structure of the anticyclonic gyres found in the Alboran Sea. *Journal of Geophysical Research*, **95**, 1599–1613.
- HOLLOWAY P. E. (1987) Internal hydraulic jumps and solitons as a shelf-break region on the Australian North West Shelf. *Journal of Physical Oceanography*, **14**, 1787–1799.
- LEVINE M. D. and J. G. RICHMAN (1989) Extracting the internal tide from data: methods and observations from the mixed layer dynamics experiment. *Journal of Geophysical Research*, **94**, 8125–8234.
- OU H. W. and L. R. M. MAAS (1988) Tides near a shelf-slope front. *Continental Shelf Research*, **8**, 729–736.
- PERKINS H., T. KINDER and P. E. LAVIOLETTE (1990) The Atlantic inflow in the Western Alboran Sea. *Journal of Physical Oceanography*, **20**, 242–263.
- RICO J. and A. RUIZ (1988) Fluctuaciones del flujo en el Estrecho de Gibraltar. *Proceedings workshop on Physical Oceanography of the Strait of Gibraltar*, Madrid.
- SMYTH N. F. and P. E. HOLLOWAY (1988) Hydraulic jump and undular bore formation on a shelf break. *Journal of Physical Oceanography*, **18**, 947–962.
- SVERDRUP H. U., M. W. JOHNSON and R. H. FLEMING (1942) *The oceans*. Prentice-Hall, Englewood Cliffs, New Jersey, 1087 pp.
- WATSON G. and I. S. ROBINSON (1990) A study of internal wave propagation in the Strait of Gibraltar using shore-based marine radar images. *Journal of Physical Oceanography*, **20**, 374–395.